Acta Geochim (2024) 43:87–96
https://doi.org/10.1007/s11631-023-00643-5

ORIGINAL ARTICLE

Facies development and sedimentology of the Middle Miocene carbonates of the Raghama Formation, northeastern Saudi Arabia

Mansour H. Al-Hashim[1] · Abdelbaset S. El-Sorogy[1] · Meshal Wadani[1]

Received: 25 March 2023 / Revised: 7 September 2023 / Accepted: 26 September 2023 / Published online: 3 October 2023

Abstract Ragahama Formation comprises a siliciclastic continental deposits followed by marine carbonates, representing prograding alluvial fans from adjacent high hinterlands seaward into lagoons and fringing reef environments. The present work aimed to document the facies development and sedimentology of the Raghama carbonates exposed along the eastern coastal plain of the Red Sea, northwestern Saudi Arabia. Four stratigraphic sections were measured and sampled (D1–D4) and thin sections and major and trace element analyses were prepared and applied for petrographic and geochemical approaches. The carbonates were subdivided into three successive fore-reef, reef-core, and back-reef depositional facies. Sandy stromatolitic boundstone, microbial laminites, dolomitic ooidal grainstone, bioclastic coralline algal wackestone, sandy bioclastic wackestone, and coral boundstones were the reported microfacies types. Petrographic analysis reveals that the studied carbonates were affected by dissolution, dolomitization, and aggrading recrystallization, which affects both the original micrite matrix and grains or acts as fracture and veinlet filling leading to widespread vuggy and moldic porosity. No evidence of physical compaction, suggesting rapid lithification and recrystallization during early diagenesis and prior to substantial burial and intensive flushing by meteoric waters. Most of the original microstructure of corals were leached and destructed. This is indicated by the higher depletion in Sr and Ca levels and increase in Mg, Na, Fe, and Mn levels, especially in section D1, in comparison with the worldwide carbonates.

Keywords Raghama Formation · Miocene · Diagenesis · Geochemistry · Saudi Arabia

1 Introduction

Diagenetic processes affect sediments immediately after deposition up until low metamorphism commences, resulting in textural and geochemical alterations in the affected rocks (Bathurst 1975; Cochran et al. 2010). These processes take place in different diagenetic zones (e.g., marine, meteoric, and burial) and under a wide range of depositional settings and conditions. Furthermore, one or more diagenetic processes (e.g., compaction, micritization, dissolution, and cementation) may act simultaneously, and more than one diagenetic phase may be recognized in the same limestone sample that has experienced different diagenetic regimes. Marginal and shallow marine carbonate sequences, for instance, may be subject to extensive meteoric and shallow marine diagenesis resulting in diagenetic textures that may later be overprinted by deep burial diagenetic features (Braithwaite and Camoin 2011; Ren and Jones 2016). What complicates the matter even further is the fact that diagenetic processes are controlled by a complex interplay of different parameters such as the primary mineralogy and texture of the sediments as well as their pore-water chemistry and the tectonic evolution of the sedimentary basin within which they were deposited (Seibel and James 2017; Morad et al. 2019).

Deciphering the diagenetic history of carbonate rocks is thus not a straightforward task, and requires the utilization

✉ Mansour H. Al-Hashim
malhashim@ksu.edu.sa

[1] Department of Geology and Geophysics, College of Science, King Saud University, 2455, Riyadh 11451, Saudi Arabia

of different observational and analytical tools. The best reconstruction of the diagenetic history of limestones is obtained via an integrated approach that combines different aspects of the rocks including petrographic characteristics and elemental and isotopic geochemical properties (Budd and Land 1990; Coimbra et al. 2018; Adefris et al. 2020). For example, textural diagenetic alterations can be detected and evaluated via different methods including petrographic analysis, X-ray diffraction (XRD), and scanning electron microscopy (SEM) (McGregor and Gagan 2003; Booker et al. 2020). However, subtle diagenetic alterations of the chemistry of carbonate rocks, which may not necessarily be manifested as textural changes, necessitate the utilization of other techniques such as the geochemical analysis of major and trace elemental concentrations and ratios of carbonate rocks (Booker et al. 2020).

Unlike the Middle Miocene deposits exposed in the western side of the Red Sea and the Gulf of Suez in Egypt which have received much attention (e.g., El-Sorogy and Ziko 1999; El-Sorogy 2015; Tawfik et al. 2015; El-Sorogy et al. 2017), their counterparts along the eastern side of the Red Sea of Saudi Arabia have relatively got less attention most of which was driven by the economic potential of the area (e.g., Cole et al. 1995; Tubbs et al. 2014; El-Sorogy et al. 2020). Furthermore, the few studies previously conducted on the Miocene occurrences along the Red Sea of Saudi Arabian were mainly focused on the paleontological and sedimentological aspects of the rocks (Hughes and Johnson 2005; Hughes 2014; Koeshidayatullah et al. 2016). The majority of these studies focused on the regional geology, paleoecology, and stratigraphy of Midyan region deposits (e.g., Hughes et al. 1999; El-Sorogy et al. 2020). None of the previous studies were conducted on the Middle Miocene exposures between Duba and Almuwaylih cities on the NE part of the Red Sea (Fig. 1), which are the focus of the current investigation. The only exception was the investigation carried out by Tawfik et al. (2021) where the authors reported a detailed lithofacies analysis within a sequence stratigraphic framework of the study area. The main objective of this study is to document the facies development, diagenetic, and geochemical investigations of the Middle Miocene carbonates of the Raghama Formation, exposed in the northwest of Saudi Arabia using an integrated field, petrographic and geochemical investigations. The obtained results are utilized in the characterization of the depositional environments and the assessment of diagenetically driven textural and compositional alterations.

2 Geological setting

The name Ragahama was initially assigned to Tertiary rocks exposed along the eastern coast of the Gulf of Aqaba (Bramkamp et al. 1963; Brown et al. 1963) before it was later exclusively used to describe Miocene successions exposed along the eastern coastal plain of the Red Sea (Powers et al. 1966). The type section of the Ragahama Formation is located at Jabal ar Raghamah in the Ash Shifa region east of the Gulf of Aqaba. According to the United States Geological Survey (USGS 1963), Miocene rocks exposed in northwestern Saudi Arabia, which includes the current study area, are divided into lower continental deposits mainly of siliciclastic deposits, middle littoral and marine deposits, and upper clastics (Tawfik et al. 2021). Similar lithostratigraphic succession was recognized in the study area, with the exception that the uppermost part of the upper clastics is assigned here to the Pliocene rather

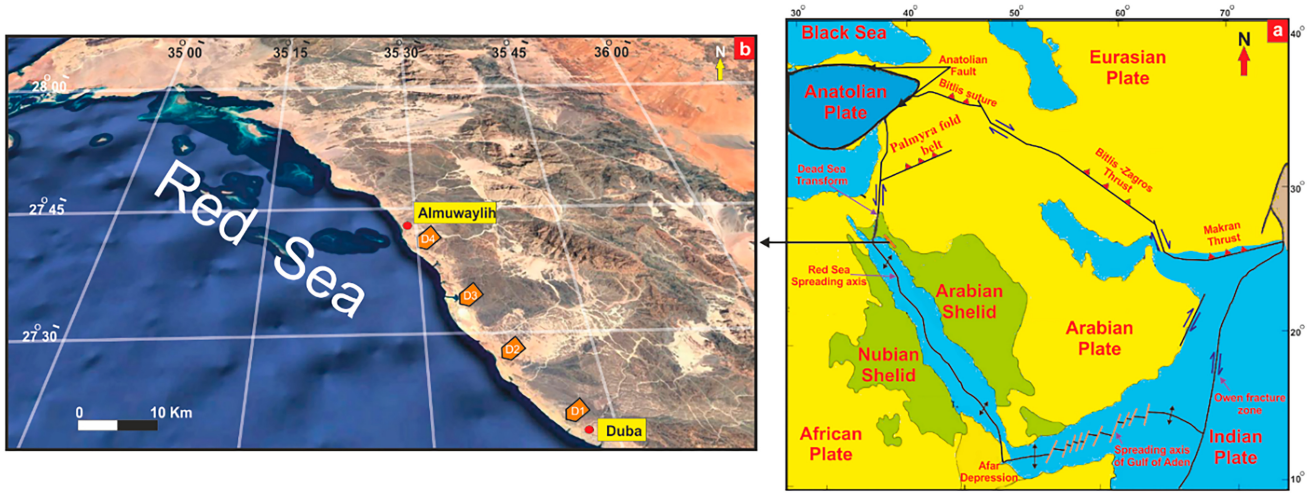

Fig. 1 Study area map showing the location of the four studied Raghama sections (D1–D4) between Duba and Almuwaylih cities along the Red Sea coast of Saudi Arabia. (Modified from Tawfik et al. 2021)

than the Miocene. Throughout the study area, the formation unconformably overlies Precambrian basement rocks or locally overlying the Cretaceous to Oligocene sedimentary succession of Azlam Formation and is unconformably onlapped by Pliocene clastics (Tawfik et al. 2021). The formation attains a total thickness of 55 m and can be divided into a lower part of mostly continental clastic deposits and an upper part of lagoonal and shallow marine carbonate rocks, collectively representing prograding alluvial fans from adjacent high hinterlands seaward into lagoons and fringing reef environments.

The Red Sea is part of a greater rift system that represents a perfect model for the transition and evolution of a continental lithospheric rifting into oceanic seafloor spreading (i.e., an ocean in the making) (Bosworth 2015). This rift system includes the Gulf of Aden, the Afar region, the Red Sea, and the Gulf of Aqaba and Suez (Bosworth 2015). Tow-rifting stages have led to the formation of the Red Sea. The first stage comprised the doming and continental rifting of the Arabian–Nubian shield that took place during the Late Oligocene to Middle Miocene, following rifting of the Gulf of Aden and Afar region (Rasul et al. 2015; Stockli and Bosworth 2019). The initial rifting was the result of reactivation of Precambrian structural weakness zones and pre-existing, steeply dipping fault systems within the Arabian–Nubian shield, which is a Neoproterozoic (870–560 Ma) accretion of ancient island arc and back-arc basins as well as continental microplates and ancient oceanic basins all of which were welded together during the Proterozoic Pan-African Orogeny (Stern 1994; Ghebreab 1998; Bosworth et al. 2005; Ligi et al. 2015). The second stage was the further rifting and spreading of the Red Sea trough which may have occurred during the past 10 Ma (Rasul et al. 2015).

Following initial rifting, local uplift of isolated fault blocks ensued along the northern Red Sea margin of Saudi Arabia, and syn-rift strata represented by Al Wajh Formation at the Midyan region were deposited (Bosworth et al. 2005). These strata consist of fluvial-lacustrine siliciclastic deposits and are overlain by laterally extensive evaporite and carbonate strata of the Tayran Group, which probably represents a sea-level fall (Bosworth et al. 2005; Koeshidayatullah et al. 2016). Near the end of the initial rifting was marked by the development of carbonate platforms of the northern Red Sea which was facilitated by the coalescence of the individual fault blocks and the formation of larger half grabens (Bosworth et al. 2005). Further subsidence of the main rift and footwall uplift led to the establishment of fully open marine conditions as evidenced by the presence of Globigerina-rich shales and deepwater limestones on top of evaporite and carbonate strata (Bosworth et al. 2005). In the Midyan region, deep marine strata are represented by the Burqan Formation (Koeshidayatullah et al. 2016). Due to the extension and concomitant marginal uplift both of which are associated with the rifting process, Neoproterozoic (550–900 Ma) (Stern and Kroner 1993) basement complexes of ultramafic, metavolcanic, and metasedimentary rocks were exposed along the Nubian and Arabian rift margins of the Red Sea. These rocks which are intruded by basalt, rhyolite, and dolerite dikes (Hughes and Johnson 2005) bound the study area in the north and the northeast.

3 Methods

A total of 75 carbonate rock samples have been collected from four stratigraphic sections of the Raghama Formation exposed in the area between Duba and Almuwaylih: D1 (27°22′14″ N, 35°39′52″ E), D2 (27°28′20″ N, 35°35′17″ E), D3 (27°34′10″ N, 35°34′03″ E), and D4 (27°39′33″ N, 35°30′05″ E) (Fig. 1). Specifically, the carbonate hand specimens were collected from the upper part of the formation which mainly consists of lagoonal carbonates and fringing reef deposits (Fig. 2). In order to evaluate diagenetic textural effects, 40 thin sections were studied by standard petrographic techniques. The distinction between calcite and dolomite was accomplished by staining the thin sections with Alizarin Red S (following Dickson 1965). In addition, 29 carbonate samples were prepared for major and trace element concentrations, including Ca, Mg, Fe, Mn, Na, and Sr. Sample preparation and geochemical analyses were conducted using Inductively Coupled Plasma Mass Spectrometry (ICP–MS) at the Geoscience Laboratories of the Ontario Ministry of Energy, Northern Development and Mines, Sudbury, Ontario, Canada.

4 Results

4.1 Facies definition and development

On the basis of field observations, microfacies analysis and associated megafossils, the studied carbonates were subdivided into three successive depositional facies which include fore-reef, reef-core, and back-reef.

The fore reef facies in the study area disconformably overlay the clastic sediments of the Raghama Formation and are represented by 6 m thick sandy coralline boundstone and microbial laminites, with rhodolith of red algae, and domal and heads of scleractinian corals of *Favites, Tarbellastraea, Porites, Thegioastraea* spp., as well as echinoids, algae, bivalves, and miliolids. Red algae play an important role in binding and connecting the coral colonies and other constituents into a coherent mass. Coralline

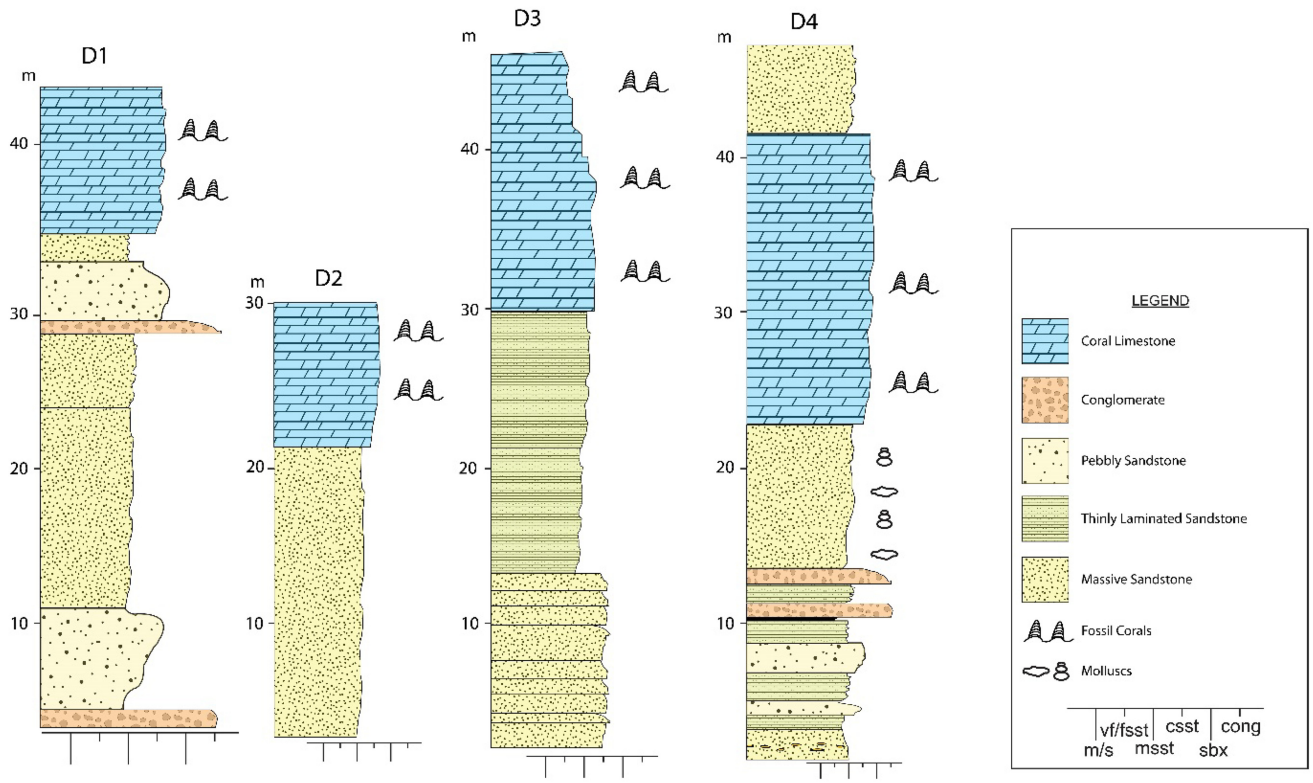

Fig. 2 Simplified stratigraphic sections of the of the four studied Raghama sections (D1–D4).

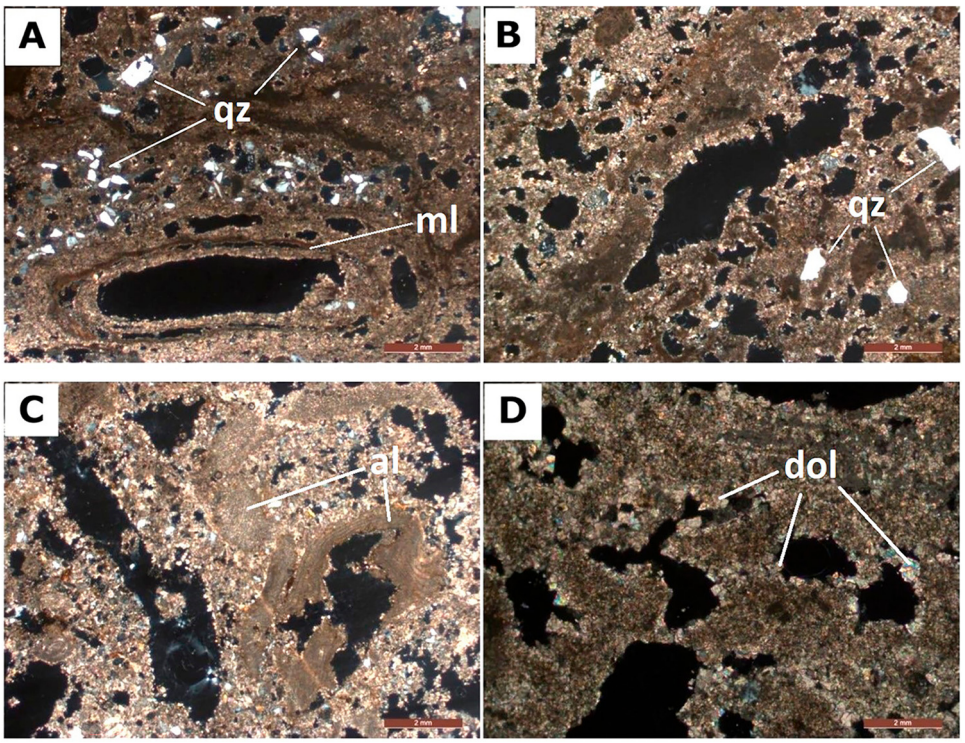

Fig. 3 Microfacies types of the fore reef unit. **A**, **B** Sandy algal framestone and microbial laminites (ml) characterized by either void of filling or filled with monocrystalline quartz sand grains (qz). **C** Bioclastic packestone with algal fragments (al) with very fine quartz grains, **D** the coarsely, blocky dolomitization (dol)

framestone, sandy algal framestone, coralline rudstone, and sandy bioclastic packestone were the microfacies representatives of this unit (Fig. 3). Some subangular, monocrystalline sand quartz grains are disseminated within coral skeletons.

The reef core is up to 24 m thick and consist of very hard, bioturbated coralline limestones that are especially well preserved in D4 (Fig. 4B) The recognized corals are massive and columnar colonies of *Porites* sp., *Favites* sp.; *Stylophora* sp., *Montastrea* sp., and *Heliastraea* sp., with encrusting *Lithothamnion* sp. and *Archaeolithothamnion* sp., which suggest deposition in a warm, shallow subtropical marine environment (Tawfik et al. 2021). Microfacies types are represented by sandy scleractinian framestone, microbial laminites, dolomitic ooidal grainstone, bioclastic coralline algal wackestone (Fig. 5).

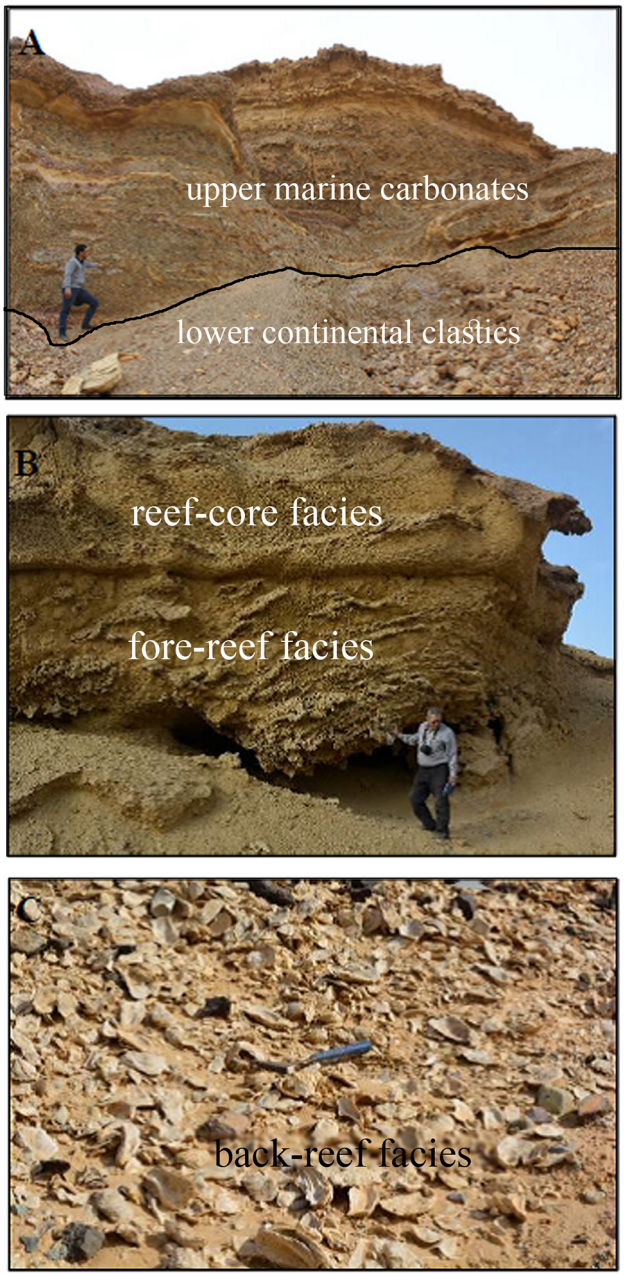

Fig. 4 **A** general outcrop view of the Raghama Formation showing the two major subdivisions of the formation; **B** the upper part of the formation consisting of reefal limestone; **C** oyster bed of *Crassostrea gryphoides* represents back-reef depositional facies in the uppermost part of the sequence

The back-reef depositional facies is represented in the study area by 1.5–2 m thick, yellowish-white friable limestone flooded with *Crassostrea gryphoides* and scattered coral colonies which terminated the carbonate sequence in D4 section (Fig. 4C). From microfacies point of view, the back-reef is represented by coralline wackestone and sandy algal grainstone. The presence of clastic sediments within back-reef facies indicated transportation during storms and rainy periods (El-Sorogy and Ziko 1999). The larger-sized shells of *C. gryphoides* allowed settlement of many bioeroder such as *Entobia*, *Gastrochaenolites*, *Caulostrepsis*, *Maeandropolydora*, and *Oichnus* ichnospecies. The presence of such benthic ichnofacies community indicated clear, agitated, and oxygenated waters, with a low rate of sedimentation.

4.2 Diagenetic and geochemical investigations

The lower fore reef part of the succession is affected by dissolution, leading to widespread vuggy porosity, and by recrystallization and partial dolomitization of the original micrite matrix (Fig. 3D). The dolomite is in the form of anhedral fine crystalline but coarsely crystallized blocky euhedral forms were noted as well, forming an idiotopic mosaic texture (Fig. 5A, B, D). The dolomite was also found to act as fracture filling. It has been observed, however, that recrystallization is minimal in samples of D1 and it progressively intensifies through to D4, where the entire samples are coarsely recrystallized with total obliteration of the original matrix and laminites. The dolomitic ooidal grainstone unit is affected by partial to complete dissolution as well as recrystallization, but with no evidence of physical compaction (Fig. 5A, B), suggesting rapid lithification and recrystallization during early diagenesis and prior to substantial burial. The studied samples are highly recrystallized in D2 and partially recrystallized in D3 but with evident extensive dissolution effects in the latter (Fig. 5A). When not completely obliterated, relict and ghost ooids display concentric internal structures (Fig. 5B).

Coral skeletons are also affected by partial dissolution (D2 and D4 sections). The coral framework on the topmost of the studied sections is composed of micrite with obvious dolomitization and aggrading recrystallization (Fig. 6B–D). Recrystallization seems to spread from within the

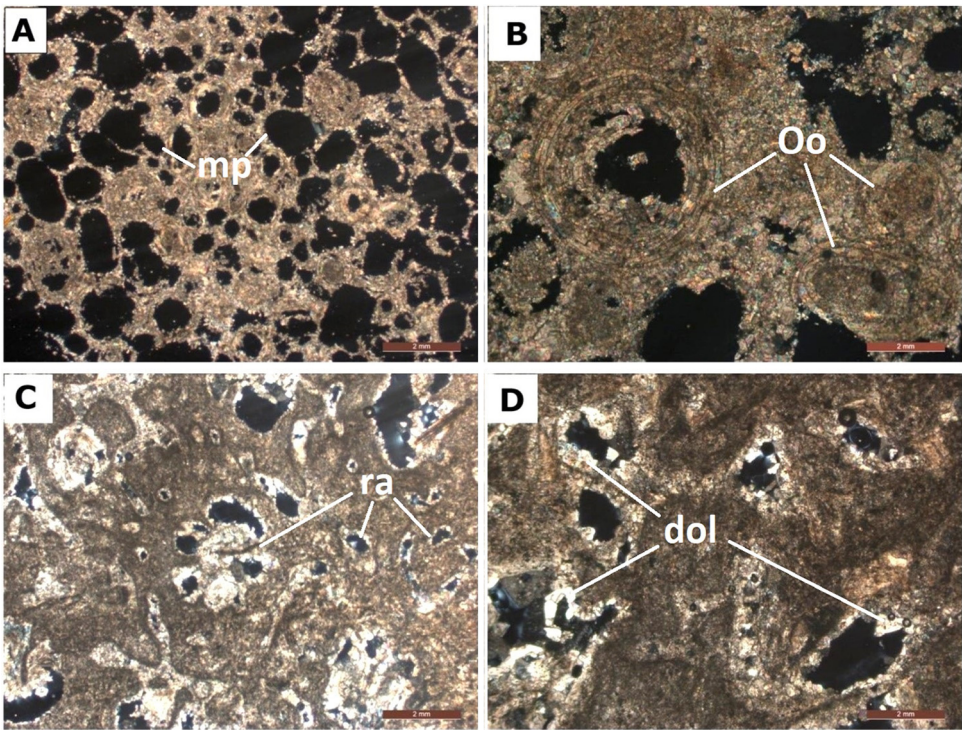

Fig. 5 Microfacies types of the reef core unit. **A**, **B** Dolomitic ooidal grainstone showing moldic porosity (mp) and partial to complete dissolution and recrystallization of ooids (Oo). **C**, **D** Bioclastic coralline algal wackestone characterized by encrusting rhodolith red algae (ra) and dolomitization (dol) with dolomite crystals becoming coarser around void marginsyuio

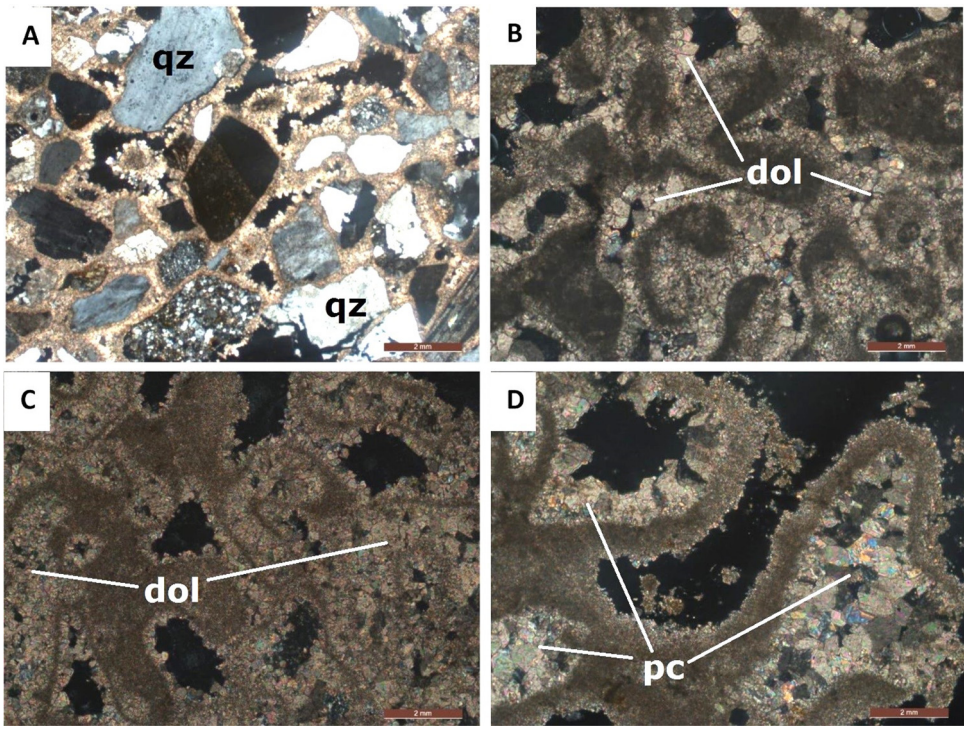

Fig. 6 Photomicrographs showing carbonate rocks from the top of the studied sections: **A** sandy bioclastic wackestone with abundant quartz grains (qz). **B**, **C** coral boundstone affected by dolomitization (dol) and by recrystallization in the form of prismatic and equant calcite (pc) (**D**)

coralline walls (Fig. 6D). Coral skeletons were completely destructed during dissolution and precipitation of low-Mg calcite by a concomitant process, with preservation of few dark centers of sclerodermites (Fig. 6B–D).

Table 1 presents a comparison between the average concentrations of Ca, Mg, Sr, Na, Fe, and Mn from carbonates of the studied sections and those from the global references of carbonates, crustal average, and earth's crust (Turekian and Wedepohl 1961; Taylor 1964; Yaroshevsky 2006). Our average Ca values were greater than those reported from the crustal average, and the Earth's crust. The average values of D1and D3 were lower than the

global references of carbonates (Turekian and Wedepohl 1961). The highest Mg Average value is reported in D1 (9.22%) in comparison with the remaining studied sections and the global references. Average values of Ca and Sr had the following descending order: D2 > D4 > D3 > D1, while Mg and Mn had the following descending order: D1 > D3 > D4 > D2 (Table 1). The low Sr content along with high Fe and Mn contents in section D1 is supported by the positive relationships between Fe and Mn (Fig. 7), and the strong negative (inverse) relationships between the amount of Ca and the concentration of Fe in the analyzed samples (Fig. 8). The high Na content in our sections in comparison with the carbonates of Turekian and Wedepohl (1961) is attributed to contamination from siliciclastic components which explains the sandy nature of the carbonate samples. This high variability of Fe and Mn con-

Table 1 Average values of the major and trace elemental concentrations in carbonates of the form the Raghama Formation, along with some background references

Location and reference	Ca (%)	Mg (%)	Sr (ppm)	Na (ppm)	Fe (ppm)	Mn (ppm)
Present study						
D1 (average)	18.46	9.22	216.88	4022.2	8788. 9	2222.2
D2 (average)	37.65	0.2	878.72	472.72	2309.09	281.81
D3 (average)	26.79	1.15	569.37	4512.5	21212.5	862.5
D4 (average)	33.94	0.317	736.77	2266.67	3766.67	311.11
Turekian and Wedepohl (1961) for carbonates	30.23	4.7	610	400	3800	1100
Taylor (1964) for crustal average	4.15	2.33	375	23,600	56,300	950
Yaroshevsky (2006) for Earth's crust	2.96	1.87	340	25,000	46,500	1000

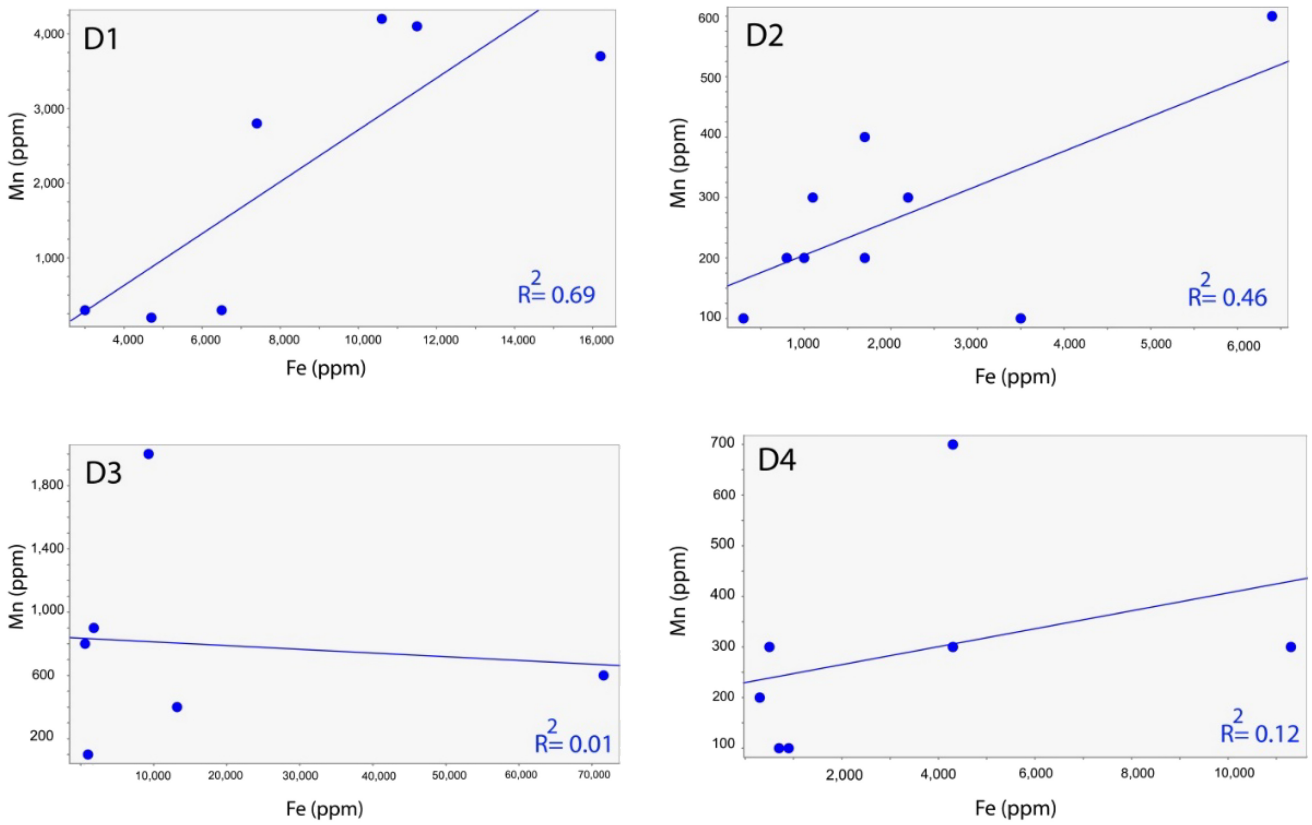

Fig. 7 Scatter diagrams showing positive relationships between Fe and Mn in the studied sections

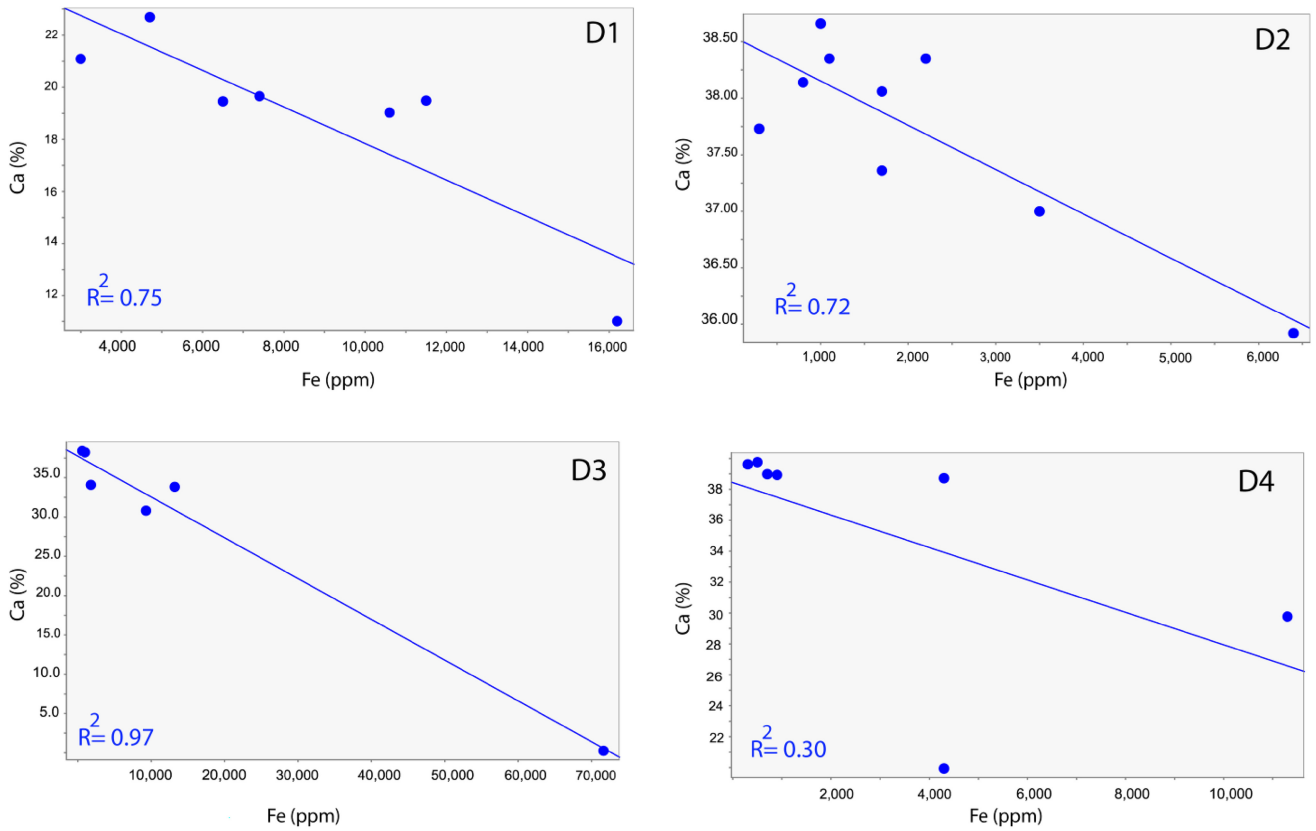

Fig. 8 Scatter diagrams showing strong, negative (inverse) relationships between Ca content and Fe concentration in the studied sections

centrations in section D3 samples explains the lack of a clear positive relationship between the two elements (Fig. 7).

5 Discussion

An age of Early to Middle Miocene was assigned to the Ragahama Formation based on reported fossil assemblages such as foraminifera (*Borelis melo*), corals (*Lithophyllia michelotti*), echinoids (*Clypeaster latirostris, Echinodiscus desori*), and bivalve (*Ostrea digitate*) (Tawfik et al. 2021). Tectonic constraints such as raised coral reefs and escarpments uplift further attest to the proposed age frame for the Ragahama Formation in the study area (Spencer 1987). However, the studied reefal limestone is equivalent in Egypt to the Nullipore limestone of the Hammam Faraun Member, Belayim Formation, Gulf of Suez (Moon and Sadek 1923), and the Early to Middle Miocene carbonate succession at Gebel Safra, southern Sinai (Abu-Elenain and El-Sorogy 1994). Also it can be correlated to the Langhian reefal limestone at Gebel Gharra, northwest Gulf of Suez (El-Safory and El-Sorogy 1999); at Wadi Hagul, Cairo-Suez District (El-Sorogy and Ziko 1999) and the late Early to Middle Miocene coral reefs in Gebel Abu Shaar El-Qibli, Red Sea coast (El-Sorogy 2001). Moreover, it is correlated with the Middle Miocene reefal limestone of Wadi Waqb Member, Jabal Kibrit Formation (Al-Kahtany 2017; El-Sorogy et al. 2020).

The presence of quartz and feldspar grains of igneous origin (Fig. 6A) within coral colonies indicates rainy periods, which transported them from the hinterland mountains (Kahal et al. 2019). Such carbonate body was deposited most probably in a shallow shelf lagoon with open circulation, just below the wave base in facies belt 7 (Wilson 1975; Abu-Elenain and El-Sorogy 1994).

The higher depletion in strontium and calcite in the studied section and the increasing Mg and Mn concentration levels are attributed to the complete destruction of coral skeletons during diagenetic processes. Furthermore, the high Fe and Mn contents in section D1 indicate the extent of diagenetic alteration, mostly in the form of dolomitization (Veizer 1983); and via remobilization and concentration of both Fe and Mn during high-Mg calcite stabilization and dissolution. The variable and high Fe content in D1 is possibly explained by dolomitization, which has also been observed in thin sections, and the concentration of iron in the lattice of coarse diagenetic calcite crystals (sparite). It may also be due to local

variation in the fluid-rock interactions and meteoric diagenesis (Al-Ramdan 2017).

The transition from clastic to non-clastic rocks in the Raghama Formation represents the maximum flooding surface (Tawfik et al. 2021). The accommodation space continued to grow, and the carbonates were formed during sea-level highstands, which were thick in sections D4 and D3, in comparison to sections D2 and D1 (Fig. 2). The continued rise in sea level during the early stage of the highstand system tract (HST) led to the flourishing of marine fossils, especially fringing reefs, which indicate eustatic and climate effects of tropical to subtropical temperature in a normal salinity fully marine setting (Abu-Elenain and El-Sorogy 1994; El-Sorogy et al. 2020).

In the last stage of the HST, the subsidence had begun as a result of widening the Red Sea, and the accommodation space was limited due to eustatic sea-level fall, as a result, the corals and other fossils had declined toward the top. Sea-level fall and forced regression are based on the deposition of oyster bed (*C. gryphoides*) in a back-reef depositional facies with a low sedimentation rate terminated the carbonate sequence in D4 section (Fig. 4C). As a result of the continuity of sea-level fall, carbonates (highstand sediments) were exposed, and disconformity was created between the Miocene and the sandy Pliocene rocks.

6 Conclusions

The present study highlighted the facies, diagenetic, and geochemical approaches of the Middle Miocene Raghama carbonates, Red Sea coast, Saudi Arabia. The following were the important findings:

1. The carbonate succession is divided into three successive fore-reef, reef-core, and back-reef depositional facies in the four studied sections. Skeletal boundstones, grainstones, and wackestones were the recorded microfacies types, with algal, coral, and other reefal fragments.
2. Dissolution, dolomitization, and aggrading recrystallization were the diagenetic processes affecting both the original micrite matrix and skeletal grains leading to leaching and destruction of the original microstructure of corals and consequently widespread vuggy and modic porosity.
3. Presence of detrital materials of igneous origin among coral colonies might indicate rainy periods, which transported them from the hinterland mountains. The intensive flushing by meteoric waters is indicated by the higher depletion in Sr and Ca levels, and increase in Mg, Na, Fe, and Mn levels, especially in section D1, in comparison with the worldwide carbonates.
4. Field observations, microfacies analysis, and faunal content, combined with trace element composition revealed that the carbonates of the Ragahama Formation were deposited in shallow shelf lagoon, winnowed platform edge and organic reef build-up environments.

Funding This research was supported and funded by the Researchers Supporting Project number (RSPD2023R781), King Saud University, Riyadh, Saudi Arabia.

Declarations

Conflict of interest The authors certify that neither the submitted material nor portions thereof have been published previously or are under consideration for publication elsewhere. The authors declare that they have no known competing financial interests or personal relationships that could have appeared to influence the work reported in this paper.

References

Abu El-Enain F, El-Sorogy AS (1994) Microfacies, depositional environments and geochemistry of the Miocene carbonate succession of Gabal El-Safra, southern Sinai, Egypt. Middle East Res Center Ain Shams Univ Earth Sci Ser 8:167–177

Adefris D, Nton ME, Boboye OA, Atnafu B (2020) Petrography and stable oxygen and carbon isotopic composition of the Antalo Limestone, Mekelle Basin, Northern Ethiopia: implications for marine environment and deep-burial diagenesis. Carbonates Evaporites 35:124

Al-Kahtany KM (2017) Facies development of the Middle Miocene reefal limestone in Northwest Saudi Arabia. J Afr Earth Sci 130:134–140

Al-Ramadan K (2017) Geochemical signatures of pervasive meteoric diagenesis of Early Miocene syn-rift carbonate platform, Red Sea, NW Saudi Arabia. Geol Q 61(1):239–250

Bathurst RC (1975) Carbonate sediments and their diagenesis. Elsevier, Amsterdam, p 658

Booker S, Jones B, Li L (2020) Diagenesis in Pleistocene (80 to 500 ka) corals from the Ironshore formation: implications for paleoclimate reconstruction. Sed Geol 399:105615

Bosworth W (2015) Geological evolution of the Red Sea: historical background, review, and synthesis. In: Rasul NM, Stewart IC (eds) The Red Sea. Springer, Berlin, pp 45–78

Bosworth W, Huchon P, McClay K (2005) The Red Sea and Gulf of Aden basins. J Afr Earth Sci 43(1–3):334–378

Braithwaite CJR, Camoin GF (2011) Diagenesis and sea-level change: lessons from Moruroa, French Polynesia. Sedimentology 58:259–284

Bramkamp RA, Brown GF, Holm DA, Layne NM Jr (1963) Geologic map of the Wadi as Sirhan quadrangle, Kingdom of Saudi Arabia. U.S. Geological Survey, p 200–A

Brown GF, Jackson RO, Boogue RG, Elberg EL (1963) Geologic map of northwestern Hijaz quadrangle: U.S. Geological Survey Miscellaneous Geologic Investigations Map 1–204A, 1:500000 scale

Budd DA, Land LS (1990) Geochemical imprint of meteoric diagenesis in Holocene ooid sands, Schooner Cays, Bahamas: correlation of calcite cement geochemistry with extent ground waters. J Sediment Petrol 60:361–378

Cochran JK, Kallenberg K, Landman NH, Harries PJ, Weinreb D, Turekian KK, Beck AJ, Cobban WA (2010) Effect of diagenesis

on the Sr, o, and C isotope composition of late cretaceous mollusks from the western interior seaway of North America. Am J Sci 310:69–88

Coimbra R, Azeredo AC, Cabral MC (2018) Cretaceous coastal lagoon facies: geochemical insights into multi-stage diagenesis and palaeoclimatic signals. Cretac Res 85:60–77

Cole GA, Abu-Ali MA, Coiling EL, Halpern HI, Carrigan WJ, Savage GR, Scolaro RJ, Al-Sharidi SH (1995) Petroleum geochemistry of the Midyan and Jaizan basins of the Red Sea, Saudi Arabia. Mar Pet Geol 12(6):597–614

Dickson JAD (1965) A modified staining technique for carbonates in thin section. Nature 205:587

El-Safory Y, El-Sorogy AS (1999) Early Miocene Bryozoa of Gebel Gharra, Northwest Gulf of Suez, Egypt. Egypt J Geol 44:19–35

El-Sorogy AS (2001) Miocene coral reefs of the northern Red Sea coast, Egypt: facies development and diagenesis. Middle East Research Center, Ain Shams University. Earth Sci Ser 15:184–199

El-Sorogy AS (2015) Bryozoan nodules as a frame-builder of bryzoan microreef, Middle Miocene sediments, Egypt. J Earth Sci 26(2):251–258

El-Sorogy AS, Abd-Elmoneim M, Mowafi A, Al-Kahtany K, Gahlan H (2017) Facies analysis and biostratigraphy of the miocene sequence, Cairo–Suez District, Egypt. J Earth Sci 28(1):1–8

El-Sorogy AS, Tsaparas N, Al-Kahtany K (2020) Middle Miocene corals from Midyan area, Northwestern Saudi Arabia. Geol J 55(7):5594–5605

El-Sorogy AS, Ziko A (1999) Facies development and environments of Miocene reefal limestone, Wadi Hagul, Cairo–Suez district, Egypt. Neues Jahrbuch für Geologie und Paläontologie 4:213–226

Ghebreab W (1998) Tectonics of the Red Sea region reassessed. Earth Sci Rev 45:1–44

Hughes GW (2014) Micropalaeontology and palaeoenvironments of the Miocene Wadi Waqb carbonate of the northern Saudi Arabian Red Sea. GeoArabia 19(4):59–108

Hughes GW, Johnson RS (2005) Lithostratigraphy of the Saudi Arabian Red Sea. GeoArabia 10:49–126

Hughes GW, Perincek D, Grainger DJ, Abu-Bshait A, Jarad AM (1999) Lithostratigraphy and depositional history of part of the Midyan region, northwestern Saudi Arabia. GeoArabia 4:503–542

Kahal AY, El-Sorogy AS, Alfaifi HJ, Almadani S, Kassem OM (2019) Biofacies and diagenetic alterations of the pleistocene coral reefs, northwest Red Sea coast, Saudi Arabia. Geol J. https://doi.org/10.1002/gj.3503

Koeshidayatullah A, Al-Ramadan K, Collier R, Hughes GW (2016) Variations in architecture and cyclicity in fault-bounded carbonate platforms, early Miocene Red Sea rift, NW Saudi Arabia. Mar Pet Geol 70:77–92

Ligi M, Bonatti E, Rasul NMA (2015) Seafloor spreading initiation: geophysical and geochemical constraints from the Thetis and Nereus Deeps, Central Red Sea. In: Rasul NMA, Stewart ICF (eds) The Red Sea: the formation, morphology, oceanography andenvironment of a Young Ocean Basin. Springer, Berlin, Heidelberg, pp 79–98

McGregor HV, Gagan MK (2003) Diagenesis and geochemistry of Porites corals from Papua New Guinea: implications for paleoclimate reconstruction. Geochim Cosmochim Acta 67:2147–2156

Moon F, Sadek H (1923) Preliminary geological report on Wadi Gharandal area. Petrol Res Bull Cairo 9:1–40

Morad S, Al Suwaidi M, Mansurbeg H, Morad D, Ceriani A, Paganoni M, Al-Aasm I (2019) Diagenesis of a limestone reservoir (lower cretaceous), Abu Dhabi, United Arab Emirates: comparison between the anticline crest and flanks. Sed Geol 380:127–142

Powers RW, Ramires LF, Redond CD, Elberg EL (1966) Geology of the Arabian peninsula, sedimentary geology of Saudi Arabia. US Geol Surv Prof Paper 560D:147p

Rasul NMA, Stewart ICF, Nawab ZA (2015) Introduction to the Red Sea: its origin, structure, and environment. In: Rasul NMA, Stewart ICF (eds) The Red Sea: the formation, morphology, oceanography and environment of a young ocean Basin. Springer-Verlag, Berlin, p 614

Ren M, Jones B (2016) Diagenesis in limestone–dolostone successions after 1 million years of rapid sea-level fluctuations: a case study from Grand Cayman, British West Indies. Sed Geol 342:15–30

Seibel MJ, James NP (2017) Diagenesis of Miocene, incised valley-filling limestones; Provence, Southern France. Sed Geol 347:21–35

Spencer CH (1987) Provisional stratigraphy and correlation of the tertiary rocks in the Jiddah region. Ministry of the petroleum and mineral resources, deputy ministry for mineral resources open-file report BRGM-580 OF-06-17, p 37

Stern RJ (1994) Arc assembly and continental collision in the Neoproterozoic East African Orogen: implications for the consolidation of Gondwanaland. Annu Rev Earth Planet Sci 22:319–351

Stern R, Kroner A (1993) Late precambrian crustal evolution in NE Sudan: isotopic and geochronologic constraints. J Geol 101:555–574

Stockli DF, Bosworth W (2019) Timing of extensional faulting along the magma-poor central and northern Red Sea rift margin—transition from regional extension to necking along a hyperextended rifted margin. In: Rasul NM, Stewart IC (eds) Geological setting, palaeoenvironment and archaeology of the Red Sea. Springer International, Switzerland, pp 81–111

Tawfik M, Al-Hashim M, El-Sorogy AS, Alharbi T, Wadani M (2021) Coastal alluvial fans of the Raghama formation, Northern East Red Sea, Saudi Arabia. J Coast Res 37(3):1193–1203

Tawfik M, El-Sorogy AS, Mowafi A, Al-Malky M (2015) Facies and sequence stratigraphy of some Miocene sediments in the Cairo–Suez district, Egypt. J Afr Earth Sci 101:84–95

Taylor SR (1964) Abundance of chemical elements in the continental crust: a new table. Geochim Cosmochim Acta 28:1273–1285

Tubbs RE, Aly A, Fouda HG, Afifi AM, Raterman NS, Hughes GW, Fadolalkarem YK (2014) Midyan Peninsula, northern Red Sea, Saudi Arabia: seismic imaging and regional interpretation. GeoArabia 19(3):165–184

Turekian KK, Wedepohl KH (1961) Distribution of the elements in some major units of the earth's crust. Geol Soc Am Bull 72:175–192

United States Geological Survey USGS (1963) Geologic map of the Arabian Peninsula. Washington, DC: United States Government Printing Office, Map1-270-A

Veizer J (1983) Chemical diagenesis of carbonates: theory and application of trace element technique. In: Arthur MA, Anderson TF, Kaplan IR, Veizer J, Land LS (eds) Stable isotopes in sedimentary geology. SEPM short course, vol 10. SEPM Society for Sedimentary Geology

Wilson JL (1975) Carbonate facies in geologic history. Springer-Verlag, Berlin, p 456

Yaroshevsky AA (2006) Abundances of chemical elements in the Earth's crust. Geochem Int 44:48–55